

# Nanoscale

Accepted Manuscript



This is an *Accepted Manuscript*, which has been through the Royal Society of Chemistry peer review process and has been accepted for publication.

*Accepted Manuscripts* are published online shortly after acceptance, before technical editing, formatting and proof reading. Using this free service, authors can make their results available to the community, in citable form, before we publish the edited article. We will replace this *Accepted Manuscript* with the edited and formatted *Advance Article* as soon as it is available.

You can find more information about *Accepted Manuscripts* in the [Information for Authors](#).

Please note that technical editing may introduce minor changes to the text and/or graphics, which may alter content. The journal's standard [Terms & Conditions](#) and the [Ethical guidelines](#) still apply. In no event shall the Royal Society of Chemistry be held responsible for any errors or omissions in this *Accepted Manuscript* or any consequences arising from the use of any information it contains.

Submitted to *Nanoscale*, May 2015 (Revised July 2015, Second Revised August 2015, Third Revised September 2015)

## Bottom-up, Hard Template and Scalable Approaches toward Designing Nanostructured $\text{Li}_2\text{S}$ for High Performance Lithium Sulfur Batteries

Lin Chen,<sup>a,b</sup> Yuzi Liu,<sup>c</sup> Nancy Dietz-Rago<sup>d</sup> and Leon L. Shaw<sup>\*,a,b</sup>

<sup>a</sup> Wanger Institute for Sustainable Energy Research, USA

<sup>b</sup> Department of Mechanical, Materials and Aerospace Engineering, Illinois Institute of Technology, Illinois 60616, USA

<sup>c</sup> Center for Nanoscale Materials, Argonne National Laboratory, Illinois 60439, USA

<sup>d</sup> Chemical Sciences and Engineering Division, Argonne National Laboratory, Argonne, Illinois 60439, USA

### ABSTRACT

$\text{Li}_2\text{S}$  with a high theoretical capacity of 1166 mA h/g and capability to pair with lithium free anodes has drawn much attention for the lithium sulfur (Li-S) battery applications. However, the fast battery decay and low capacity retention due to dissolution of intermediate polysulfides in electrolytes limit its development. Designing a nanosized and nanostructured host for  $\text{Li}_2\text{S}$  through facile techniques is one of the ways to alleviate the dissolution and improve Li-S battery performance; nevertheless, it is technically difficult to synthesize nanosized and nanostructured hosts for  $\text{Li}_2\text{S}$  because  $\text{Li}_2\text{S}$  is highly sensitive to moisture and oxygen. Herein, a novel technique, i.e., a bottom-up, hard template and scalable method is proposed to engineer nano $\text{Li}_2\text{S}$  composites with core-shell structures as cathodes of Li-S batteries. The size of the as-prepared nanostructured  $\text{Li}_2\text{S}$  is around 100 nm. With the assistance of FETEM, HRTEM and EFTEM elemental mapping, an excellent core-shell structure has been confirmed and the outside carbon shell has a thickness of 20-50 nm, effectively retarding polysulfides outflow and dissolution. A high initial capacity of 915 mA h/g at 0.2 C has been achieved upon electrochemical cycling and

the battery still has exceptional capacity retention after prolonged 200 cycles with a limited decay of 0.18% per cycle. Also, at 0.5 C the electrode exhibits 60% capacity retention with a long life of 300 cycles. We attribute these good performances to nano-architecture constructed by the novel and facile method.

**KEYWORDS:** hard template, core-shell structure, Li<sub>2</sub>S cathodes, Li-S batteries

Corresponding author: Leon L. Shaw, [lshaw2@iit.edu](mailto:lshaw2@iit.edu)

## 1 Introduction

Rechargeable lithium ion batteries with capability of storing and delivering high energy are much attractive to reduce the emission of greenhouse gas from fossil fuel combustion.<sup>1-3</sup> Recently, batteries are also gaining attention to be electrochemical storage devices for intermittent energy,<sup>4-6</sup> such as solar energy<sup>7</sup> and wind power.<sup>8, 9</sup> They find daily life applications as well, e.g., powering wearable devices,<sup>10</sup> cellphones and electric vehicles.<sup>11</sup> However, the low theoretical capacity (274 mAh/g based on LiCoO<sub>2</sub> as cathodes) of commercial lithium ion batteries leaves little room for further development.<sup>12</sup> Thus, exploiting high energy density rechargeable cells with new chemistries,<sup>13-16</sup> i.e., going beyond lithium ion batteries, is imperative.

The lithium sulfur (Li-S) battery, as one of the most promising battery candidates, has a high theoretical capacity of 1672 mA h/g based on elemental sulfur<sup>17</sup> and delivers high specific energy density (theoretically 2500 Wh/kg sulfur).<sup>17</sup> Besides, it has advantages of low costs due to the abundance of sulfur,<sup>18, 19</sup> and environmental benignancy.<sup>20</sup> Thus, developing Li-S batteries has attracted extensive investigation in the last decades. Despite advances from previous work,<sup>14, 21-28</sup> the commercialization of Li-S batteries still has a long way to go due to suffering from some major challenges: 1) the low conductivity of sulfur based materials; 2) the volume expansion of sulfur element upon discharging processes causing the electrode pulverization; and 3) the dissolution of lithium polysulfides within liquid electrolytes, leading to loss of active materials and capacity decay.<sup>29</sup> Most importantly, the safety issue resulting from being coupled with lithium metal anodes in formation of lithium dendrites and thus fires or explosions after long cycles is a main concern.

Li<sub>2</sub>S based materials, capable of paring with lithium free anodes,<sup>30</sup> were brought up to be used as cathodes to circumvent the safety concern. To mitigate the polysulfides dissolution problem for Li<sub>2</sub>S cathodes and increase their conductivity, many research efforts have focused on constructing nanostructures to host the nanosized material,<sup>31-33</sup> including wrapping Li<sub>2</sub>S with carbon nanotubes<sup>34</sup> and graphene,<sup>35</sup> encapsulating it in a host material, such as carbon<sup>33, 36</sup> and polymer,<sup>37</sup> or making coating by atomic layer deposition.<sup>8</sup> Despite of much progress achieved, the techniques developed are either too elaborate and complicated, or the battery performance

still degrades too fast. Developments of facile and novel approaches for high performance  $\text{Li}_2\text{S}$  materials are thus highly desirable. Herein, we proposed a new bottom-up, hard template technique towards fabricating  $\text{nanoLi}_2\text{S}@C$  for promising scalable production, with achievements of good battery performance and great capacity retention after prolonged cycles. With SEM and TEM characterizations, it is shown that the size of  $\text{Li}_2\text{S}$  is around 100 nm and a 20-50 nm thickness of carbon coating is observed on  $\text{Li}_2\text{S}$ , resulting in effectively hosting polysulfides and thus leading to good capacity retention with a long cycle life.

## 2 Experimental section

### 2.1 Preparation of $\text{nanoLi}_2\text{S}@C$

Polystyrene (PS) nanoparticles have been chosen as the hard template in this study because the hard template needs to be removed before  $\text{nanoLi}_2\text{S}@C$  can serve as an effective cathode. Without removing the hard template in the core of  $\text{nanoLi}_2\text{S}@C$  the specific capacity of the  $\text{nanoLi}_2\text{S}@C$ -based cathode will be low. As will be shown later, the PS template can be removed easily during the formation of the N-doped carbon coating of  $\text{nanoLi}_2\text{S}@C$  with no need for additional processing step. The PS nanoparticles with 50 nm in diameter were purchased from Nanocs company, which was dispersed in aqueous solutions. Freeze-dry technique was used to get the PS nanoparticles for future use. 1 g commercial  $\text{Li}_2\text{S}$  (Sigma-Aldrich) was ball-milled with steel balls (10 g) for 6 hours in a SPEX machine (SPEX Mixer 8000M).

40 mg PS was dispersed in 5 mL pure ethanol in a quartz crucible and sonicated for 30 minutes, followed by being transferred to an Ar-filled glove box. 100 mg  $\text{Li}_2\text{S}$  was then added into the suspension with continued stirring until all ethanol evaporated. The material obtained was subsequently subjected to drying process in a vacuum oven at 50 °C for 6 hours. Pyrrole was then added dropwise into the dried powder before it was put into an autoclave under Ar atmosphere. Subsequently, the sealed autoclave was treated at 600 °C for 6 hours. After being cooled down, the as-prepared materials were collected and marked as  $\text{nanoLi}_2\text{S}@C$ .

### 2.2 Materials Characterization

The XRD data was collected in the 2-theta range from 10-100 degree using Bruker X2 with

CuK $\alpha$  radiation. High resolution imaging was conducted with field emission scanning electron microscope (JEOL) in Center for Nanoscale Materials (CNM) at Argonne National Laboratory. HRTEM images and EFTEM elemental mappings were obtained with Gatan vacuum transfer holder for protecting Li<sub>2</sub>S samples in field emission transmission electron microscopy (JEOL) in CNM. Samples for TEM analysis were not exposed to air during loading into the instrument.

### 2.3 Electrochemical measurements

The as-prepared nanoLi<sub>2</sub>S@C material was mixed with PVDF and carbon black (in the 70 : 15 : 15 mass ratio) in an Ar-filled glovebox to prepare electrodes with an aluminum foil as the current collector. The mass loading of the active material for assembled cells was 0.8-1 mg/cm<sup>2</sup>, and the percentage of Li<sub>2</sub>S in the as-prepared nanoLi<sub>2</sub>S@C is 86.2%. Lithium metal was used as the counter anode. The electrolyte contained 1M lithium bis(tri-fluoromethanesulfonyl)imide (LiTFSI) salt in the dimethoxyethane (DME) and 1,3-dioxolane (DOL) solvents (1:1 v/v) with the LiNO<sub>3</sub> additive (1 wt%). 20  $\mu$ l of electrolytes was used for each coin cell. The separator employed in this work is Celgard 2325. CR2032 coin cells were assembled in the glovebox for electrochemical tests. Electrochemical impedance spectroscopy (EIS) data was collected with Parstat 4000 instrument (Princeton Applied Research) in the frequency range of 1 MHz to 0.1 Hz upon the discharge state of batteries. The cycling performances were evaluated using Arbin System BT2000. All charge–discharge processes were started with a slow charge rate of 0.05 C to 4 V and then cycled between 1.6 and 3.0 V at the desired current rates.

## 3 RESULTS AND DISCUSSION

Figure 1 shows procedures for the formation of nanoLi<sub>2</sub>S@C *via* the bottom-up approach with hard templates. The polystyrene (PS) nanoparticles were obtained through freeze drying methods and then dispersed in pure ethanol. Ball milled Li<sub>2</sub>S particles were added into the ethanol solution above, followed by precipitating Li<sub>2</sub>S onto PS nanoparticles *via* evaporation of ethanol. Some pyrrole was subsequently added to the PS@Li<sub>2</sub>S powder which was then calcined at 600 °C in an Ar atmosphere. Upon heating the PS core thermally decomposed and evaporated, leaving little or no residual carbon behind (see the discussion later). The product from this bottom-up, hard template approach will be termed as nanoLi<sub>2</sub>S@C hereafter.

Field emission scanning electron microscopy (FESEM) images of pristine PS and the final product are shown in Figure 2a and 2b, respectively. The morphology of PS nanoparticles purchased is not spherical and the average size of them is about 50 nm (Figure 2a and Figure S1 in Supporting Information). The particles do not change after freeze drying techniques (Figure S1c) under SEM. Regarding nanoLi<sub>2</sub>S@C, an average size of 100 nm for the composite can be observed (Figure 2b and Figure S1d). The particle is uniform although some agglomerations of about 200 nm exist. To the best of our knowledge, such small Li<sub>2</sub>S coated by carbon or other materials has not been reported previously.<sup>33, 37-39</sup> The small size of Li<sub>2</sub>S enables reduced diffusion distance of electrons and favors for the improved conductivity and electrochemical performance in the system. Also, it is good to mention that these Li<sub>2</sub>S particles can be employed for in-situ TEM study, which prefers nanoparticles with size less than 200 nm.

Owing to their high sensitivity to moisture and oxygen, Li<sub>2</sub>S-based materials were sealed in capillary tubes for XRD measurements, and thus the tube pattern becomes the background. The pattern of the as-synthesized nanoLi<sub>2</sub>S@C displayed in Figure 2c is consistent with JCPDS Card No. 26-1188.<sup>36, 39</sup> The peak at 26.99° (2θ) corresponds to (111) facet and demonstrates the strongest intensity compared to other peaks. It is important to notice that only Li<sub>2</sub>S pattern was observed, indicating that no side reactions occurred during processing and carbon materials are amorphous in this system. Field emission transmission electron microscopy (FETEM) image of a single nanoLi<sub>2</sub>S@C particle (Figure 2d) reveals the size of 100 nm, which is consistent with the FESEM observation. It is worthy to mention that Gatan vacuum transfer holder was utilized for all samples with TEM characterization to protect them from contacting moisture and oxygen.

In order to elucidate the core-shell structure of the as-prepared material, high resolution of transmission electron microscopy (HRTEM) coupled with selected area electron diffraction (SAED) was employed. The particle in Figure 3a is a frame we used for HRTEM analysis. Inside this particle, a lot of lattice structures are visibly seen (Figure 3b). The obvious lattice in the center has an interlayer distance of 0.33 nm, corresponding to (111) facet of Li<sub>2</sub>S in XRD pattern. The lattices distances of 0.20 nm and 0.282 nm are also observed, which are consistent with (220) and (200) facets of Li<sub>2</sub>S, respectively, demonstrating that Li<sub>2</sub>S grains exist well inside the particle.

There are bright rings in SAED exhibited in Figure 3e, indicating the typical feature of the crystalline structure. The pattern shows some diffraction rings, which are in correspondence with lattice planes of (200), (220), (311) and (400) for  $\text{Li}_2\text{S}$ , further verifying the presence of  $\text{Li}_2\text{S}$  grains inside the particle. All of these analyses unambiguously reveal that  $\text{Li}_2\text{S}$  are widely presented inside of the particle and the effective precipitation technique of  $\text{Li}_2\text{S}$  from ethanol. As we further look at the image (Figure 3c), there is a visible interface within the particle, which can be attributed to the interface between the  $\text{Li}_2\text{S}$  and outer carbon shell. There are no lattices in the carbon, indicating the amorphous nature of the carbon shell. Rotating the nano $\text{Li}_2\text{S}@C$  sample in the TEM stage confirms that the outer carbon shell is indeed amorphous since no lattice images can be observed regardless of rotating angles.

TEM search for the carbon derived from the thermal decomposition of the PS inside the  $\text{Li}_2\text{S}$  core did not provide clear evidence on whether there is an inner carbon layer within the  $\text{Li}_2\text{S}$  core or not. This may be due to the challenge of imaging the innermost amorphous carbon through multiple layers of materials (i.e., the outer amorphous carbon shell and  $\text{Li}_2\text{S}$  core) with the TEM instrument or the little quantity of residual carbon left behind from thermal decomposition of PS. Previous studies<sup>40, 41</sup> have shown that PS will melt and evaporate from 340 °C to 430 °C when tested using thermogravimetric analysis (TGA) under a flowing  $\text{N}_2$  atmosphere, leaving almost no residual carbon behind. The challenge of finding the innermost amorphous carbon in our study appears to be consistent with these prior studies on thermal decomposition of PS.<sup>40, 41</sup>

The most important factor for enhanced performance of lithium sulfur batteries probably lies in the reduction of polysulfides dissolution. Therefore, an excellent carbon coating that can host sulfur-based materials is extremely desirable, and the thickness of outer layer is vital for capacity retention. We selected two areas with clear interfaces to survey and obtain such information. The thickness of carbon in the two images is 20 nm (Figure 3c) and 52 nm (Figure 3d), respectively. Notice that there are some coating areas that thicker or thinner, but the thickness of 20-50 nm is rational for all HRTEM observations.

To further confirm the carbon-coated structure, another selected particle (Figure 4a) was analyzed by energy-filtered transmission electron microscopy (EFTEM) techniques. As revealed

in the element mappings (Figure 4b and 4c), the brightness points represent corresponding positions of elements and it can be seen obviously that carbon mapping (Figure 4b) forms a circle. It looks like that  $\text{Li}_2\text{S}$  precipitated from ethanol covered the two PS particles or the two particles were gathered during the calcination process. This indicates that individual particle is around 100 nm, the size of which is consistent with SEM observation (Figure 2b). The sulfur element mapping illustrates the position of  $\text{Li}_2\text{S}$  as it is the only source of sulfur element. We can observe that  $\text{Li}_2\text{S}$  is well encapsulated by carbon in the combination image (Figure 4d), where green and red colors represent carbon and sulfur, respectively. We are not surprised to see that some carbon are mixed with  $\text{Li}_2\text{S}$  layer because TEM images are projections of materials. To further confirm that the nanostructured  $\text{Li}_2\text{S}$  materials were fabricated, we provided another set of EFTEM images in Figure S2. The results are highly accordant with these shown in Figure 4. From all of these images and above discussions, it is unambiguous that nano $\text{Li}_2\text{S}@C$  composites have been successfully synthesized *via* this bottom-up, hard template approach, and the technique we developed here is promising for facile control of nanostructures and scalable production.

Electrochemical cycling tests were conducted to evaluate performance of the nano $\text{Li}_2\text{S}@C$  material as battery cathodes at 0.2 C and 0.5 C, shown in Figure 5a and 5d, respectively. This cathode delivered a high initial specific capacity of 915 mA h/g at 0.2 C. The cells were activated by the first charge to 4.0 volt before cycling, and it is interesting to note that there is little overpotential hump at the early stage of the first charge profile (Figure S3). This is different from previous reports<sup>42, 43</sup> and the materials developed by our group.<sup>36</sup> It demonstrates that the nano $\text{Li}_2\text{S}@C$  does not have much energy barrier due to the fine particle size and uniform nitrogen-doped carbon coating. The Coulombic efficiency for the first cycle is only 78% because of side reactions, the dissolution of polysulfides and the formation of protection layer on the lithium metal, resulting in low reversible electrochemical reactions. However, the efficiency increased to > 95% after several cycles thanks to highly reversible reactions between sulfur and lithium polysulfides/sulfides. During the charge-discharge processes, there is little decay from 20<sup>th</sup> cycle to 60<sup>th</sup> cycle (Figure 5b) and then low capacity degradation is observed. We assume that this is because the protection layer (solid-electrolyte interphase, SEI) on the lithium anode was formed completely within the 20<sup>th</sup> cycles and thus the shuttle behavior was hindered so that

the battery performance was sustained. However, it is likely that the lithiation/delithiation processes beyond 60 cycles produce stress within the lithium anode, resulting in damage to SEI<sup>44</sup> and initiating gradual and small capacity decay beyond 60 cycles. Upon prolonged 200 cycles, the capacity is still maintained at 586 mAh/g and the Coulombic efficiency keeps around 96% with a limited decay of 0.18% per cycle.

In order to assess the fast rate capability of the as-synthesized materials, fresh cells were subjected to cycling at 0.5 current rate for 300 cycles. The cathode exhibits an initial capacity of 814 mA h/g and retains 485 mAh/g after 300 cycles, which yields a decent capacity retention of about 60%, as revealed in Figure 5d. To provide the direct evidence of good electrochemical performance offered by nanoLi<sub>2</sub>S@C, two additional half cells made of ball-milled Li<sub>2</sub>S and Li<sub>2</sub>S@C were fabricated and included in Figure 5d for comparison. The ball-milled Li<sub>2</sub>S in this case did not have carbon coating, but mixed with 16 wt% carbon black and 10 wt% PVDF to form the cathodes. In contrast, Li<sub>2</sub>S@C also contained a total of 16 wt% carbon in the cathodes, but was made by first ball milling a mixture of Li<sub>2</sub>S + 7.5 wt% carbon black (CB) to form a Li<sub>2</sub>S/CB composite core, followed by carbonization of pyrrole to form the carbon shell, as detailed in Ref. 36. To provide a direct comparison, the condition for carbonization of pyrrole in Li<sub>2</sub>S@C was the same as that for nanoLi<sub>2</sub>S@C in this project. As shown in Figure 5d, the specific capacity and capacity retention of the ball milled Li<sub>2</sub>S are very poor. Furthermore, the Coulombic efficiency of the nanoLi<sub>2</sub>S@C half cell is close to 100% after 10 electrochemical cycles, whereas the ball-milled Li<sub>2</sub>S half cell has a Coulombic efficiency at only about 82%, indicating significant irreversible reactions and the essential role of the carbon shell in minimizing the dissolution of polysulfides into the electrolyte during cycling.

The most interesting phenomenon in Figure 5d is that Li<sub>2</sub>S@C has a higher initial specific capacity than nanoLi<sub>2</sub>S@C because of the CB networks inside the Li<sub>2</sub>S composite core which allow most Li<sub>2</sub>S to participate in electrochemical reactions.<sup>36</sup> However, nanoLi<sub>2</sub>S@C has much better capacity retention than Li<sub>2</sub>S@C because of a more uniform carbon shell in nanoLi<sub>2</sub>S@C made possible by the PS hard template approach. Thus, the present study provides a direct and unambiguous evidence that the quality of the carbon shell is of paramount importance in minimizing polysulfides dissolution and improving cycle stability. Finally, it should be pointed

out that the capacity retention exhibited by nanoLi<sub>2</sub>S@C is also better than multiple recently published reports<sup>8, 18, 34, 46</sup> (Figure S5), and comparable with several others with the similar mass loading and current rates<sup>31, 37, 38</sup>. More detailed discussions can be found in supporting information.

The rate capability of the nanoLi<sub>2</sub>S@C cathode material by subjecting nanoLi<sub>2</sub>S@C half cells to different charge/discharge rates (Figure 5e) is also examined. In the first 10 cycles at the 0.2 C rate, the specific capacity decreases gradually. However, the capacity does not drop much in the following charge-discharge cycles at 0.5 C and 1.0 C. In fact, when the current rate is changed to 2.0 C at the end of the 30th cycle, no more capacity decay is observed and the cell still offers a specific capacity of 501 mAh/g. All of these cyclings at high rates with good battery performance demonstrate great kinetics conditions for electrochemical reactions, thanks to the nanosized and nanostructured Li<sub>2</sub>S material with uniform N-doped carbon coating. The current rate after 40 cycles is switched back to 0.2 C and the battery performance with a specific capacity of 745 mAh/g is recovered. Interestingly, 745 mAh/g is slightly higher than the original specific capacity (738 mAh/g) at the 10<sup>th</sup> cycle before subjecting to higher current rate cycles (Figure 5e). In contrast, when Li<sub>2</sub>S@C with the similar mass loading in the cathode is subjected to the identical charge/discharge cycles with the same current rates, only 89% capacity is recovered upon switching back from 2C to 0.2 C.<sup>36</sup> These results unequivocally show the outstanding capability of the uniform carbon coating and nanosize particles enabled by the hard template approach in offering robust performance under high current rates.

To further elucidate the relationship between cycling and electrode kinetics for the nanoLi<sub>2</sub>S@C composite, electrochemical impedance spectroscopy (EIS) measurements for cells after different cycles (Figure 5c) were conducted. The Nyquist plots of all three batteries have a single depressed semicircle in the high-medium frequency region and an inclined line at the low frequency. As for the fresh cell, it does not have a complete semicircle and is fitted with a black dash line to indicate the possible position of its intercept with the real impedance axis.

The measured impedance data are fitted with the equivalent circuit displayed in the inset of Figure 5c. The elements in this equivalent circuit include four components: (i) the ohmic

resistance of the electrolyte, electrodes and any surface films on the surface of electrodes, the contact resistance at the electrolyte/electrode interfaces, and the contact resistance between the electrodes and current collectors ( $R_e$ ), (ii) the charge-transfer resistance at the electrode/electrolyte interfaces ( $R_{ct}$ ), (iii) the double layer capacitance ( $C_d$ ), and (iv) the Warburg impedance ( $Z_w$ ) related to mass transfer. Based on the fitting of this equivalent circuit, the value of  $R_e$  is  $\sim 3.7 \Omega$  for the fresh cell, and  $14.4 \Omega$  and  $14.6 \Omega$  for the cell cycled at  $0.2 C$  after 200 cycles and the cell cycled at  $0.5 C$  after 300 cycles, respectively. The fresh cell has a minimum value compared to the other two, indicating the low resistance provided by the nanostructure of nanoLi<sub>2</sub>S@C (i.e., Li<sub>2</sub>S nanoparticles with the uniform N-doped carbon coating). The increased  $R_e$  after cycling stems from the formation of the SEI layer on the anode and may also be partially due to the viscosity increase of the electrolyte caused by dissolved polysulfides during electrochemical processes.

The fitting parameter of the charge-transfer resistance,  $R_{ct}$ , is also very small ( $\sim 23 \Omega$ ) for the fresh cell. In contrast,  $R_{ct}$  increases to  $\sim 95 \Omega$  after 200 cycles and to  $\sim 123 \Omega$  after 300 cycles. The increased  $R_{ct}$  after cycles has been ascribed to the increased polarization resistance at the electrolyte/SEI interface. Based on the impedance measurement, the fresh nanoLi<sub>2</sub>S@C battery has a very small resistance synergistically induced by the fine particle size, great carbon coating and nitrogen-doped media.<sup>36, 45</sup> The electrode kinetics, therefore, in this cell is superior, consistent with the outstanding performance of the initial cycle activation with little energy barrier (Figure S3). In contrast, SEI layers were formed for cycled cells, leading to the increased equivalent series resistance ( $R_e$ ) and charge-transfer resistance at the interface ( $R_{ct}$ ).

Before closing, it should be pointed out that the practical capacity of the cathode is an important parameter. For the nanoLi<sub>2</sub>S@C cathodes in this study, the as-synthesized nanoLi<sub>2</sub>S@C contained 86.2% Li<sub>2</sub>S, and the cathodes were prepared with 70% nanoLi<sub>2</sub>S@C, 15% carbon black and 15% PVDF. In order to make direct comparison on capacity retention, Figure 6 displays the Li<sub>2</sub>S cell specific energy plot with the specific energy values estimated from recent publications, where the discharge capacity upon 100<sup>th</sup> cycle and content (%) of sulfur in the cathode are reported based on the S content (except Ref. 46 in which the 50<sup>th</sup> cycle data is used since only 50 cycles are reported by this reference). It is obvious that our sulfur content in electrode is higher than or similar to others, and our work has the best energy density over 1000

Wh/kg even after 100 cycles. This undoubtedly illustrates that great capacity retentions have been achieved by the bottom-up and template-synthesized nanoLi<sub>2</sub>S@C.

Finally, it is worthy of mentioning that the improved conductivity and electrochemical performance exhibited by nanoLi<sub>2</sub>S@C is not related to possible Fe contamination during ball milling. To rule out this possibility, we have conducted EDS measurement after nanoLi<sub>2</sub>S@C-based cathodes have been electrochemically cycled and then dismantled in a glovebox. The EDS data along with the SEM images showing the multiple locations from which the EDS data were taken are presented Figure S4 and Table S1 in Supporting Information. As shown in Table S1, no noticeable iron contamination from the ball milling process is observed. This result is consistent with our expectation since our previous study<sup>47</sup> has showed only 1.5 wt% contamination from WC balls after 75-hour ball milling in a high-energy ball milling attritor. Although in the present study steel balls were used, ball milling only lasted 6 hours. Therefore, little or no Fe contamination is consistent with our expectation.

## CONCLUSION

In summary, we report successful fabrication of nanoLi<sub>2</sub>S@C composites, for the first time, *via* a bottom-up, hard template and scalable approach. In this original and facile technique, a hard template serves as an excellent media to realize uniform deposition of nanosized Li<sub>2</sub>S, which in turn enables the formation of a superior nitrogen-doped carbon coating. As a result, the electrodes exhibit outstanding electrochemical performance with little overpotential representing energy barrier for Li<sub>2</sub>S in the initial activation process. A high initial specific capacity of 915 mA h/g at 0.2 C was yielded with only a limited decay of 0.18% per cycle with 200 cycles. The batteries also demonstrate good capacity retention of 60% after prolonged 300 cycles at 0.5 C. The good capacity retention is mainly thanks to the uniform nitrogen-doped carbon shell, which hosts polysulfides and mitigates their outflow into electrolytes. The novel strategy proposed here provides a promising way to engineer nanosized and nanostructured Li<sub>2</sub>S, paving the road for future use.

## Acknowledgements

The use of the Center for Nanoscale Materials (CNM) was supported by the U. S. Department of Energy, Office of Science, Office of Basic Energy Sciences, under Contract No. DE-AC02-06CH11357. The kindly offer of the Gatan vacuum holder for TEM and EFTEM characterization by Dr. Xiao-Min Lin at CNM is much appreciated.

*Supporting Information Available:* Additional figures and tables.

## References

1. A. Manthiram, Y. Fu and Y.-S. Su, *Acc. Chem. Res.*, 2012, **46**, 1125-1134.
2. Z.-S. Wu, W. Ren, L. Xu, F. Li and H.-M. Cheng, *ACS Nano*, 2011, **5**, 5463-5471.
3. L. Ji, Z. Lin, M. Alcoutlabi and X. Zhang, *Energy Environ. Sci.*, 2011, **4**, 2682-2699.
4. J. Lu, L. Li, J.-B. Park, Y.-K. Sun, F. Wu and K. Amine, *Chem. Rev.*, 2014, **114**, 5611-5640.
5. J. Song, Z. Yu, M. L. Gordin, S. Hu, R. Yi, D. Tang, T. Walter, M. Regula, D. Choi and X. Li, *Nano Lett.*, 2014, **14**, 6329-6335.
6. J. Liu, J. G. Zhang, Z. Yang, J. P. Lemmon, C. Imhoff, G. L. Graff, L. Li, J. Hu, C. Wang and J. Xiao, *Adv. Funct. Mater.*, 2013, **23**, 929-946.
7. V. Palomares, P. Serras, I. Villaluenga, K. B. Hueso, J. Carretero-González and T. Rojo, *Energy Environ. Sci.*, 2012, **5**, 5884-5901.
8. X. Meng, D. J. Comstock, T. T. Fister and J. W. Elam, *ACS Nano*, 2014, **8**, 10963-10972.
9. X. Su, Q. Wu, J. Li, X. Xiao, A. Lott, W. Lu, B. W. Sheldon and J. Wu, *Adv. Energy Mater.*, 2014, **4**, 1300882-1300904.
10. B. Liu, J. Zhang, X. Wang, G. Chen, D. Chen, C. Zhou and G. Shen, *Nano Lett.*, 2012, **12**, 3005-3011.
11. X. Zhu, Y. Zhu, S. Murali, M. D. Stoller and R. S. Ruoff, *ACS Nano*, 2011, **5**, 3333-3338.
12. S. Evers and L. F. Nazar, *Acc. Chem. Res.*, 2012, **46**, 1135-1143.
13. M. Pumera, Z. Sofer and A. Ambrosi, *J. Mater. Chem. A*, 2014, **2**, 8981-8987.
14. H. Wang, Y. Yang, Y. Liang, J. T. Robinson, Y. Li, A. Jackson, Y. Cui and H. Dai, *Nano Lett.*, 2011, **11**, 2644-2647.
15. H.-G. Jung, J. Hassoun, J.-B. Park, Y.-K. Sun and B. Scrosati, *Nat. Chem.*, 2012, **4**, 579-585.
16. B. Huskinson, M. P. Marshak, C. Suh, S. Er, M. R. Gerhardt, C. J. Galvin, X. Chen, A. Aspuru-Guzik, R. G. Gordon and M. J. Aziz, *Nature*, 2014, **505**, 195-198.
17. Y. Yang, G. Zheng and Y. Cui, *Chem. Soc. Rev.*, 2013, **42**, 3018-3032.
18. R. Xu, J. C. Li, J. Lu, K. Amine and I. Belharouak, *J. Mater. Chem. A*, 2015, **3**, 4170-4179.
19. M.-K. Song, E. J. Cairns and Y. Zhang, *Nanoscale*, 2013, **5**, 2186-2204.
20. L. Chen and L. L. Shaw, *J. Power Sources*, 2014, **267**, 770-783.
21. J. Schuster, G. He, B. Mandlmeier, T. Yim, K. T. Lee, T. Bein and L. F. Nazar, *Angew. Chem. Int. Ed.*, 2012, **51**, 3591-3595.
22. S. Xin, L. Gu, N.-H. Zhao, Y.-X. Yin, L.-J. Zhou, Y.-G. Guo and L.-J. Wan, *J. Am. Chem. Soc.*, 2012, **134**, 18510-18513.
23. L. Ji, M. Rao, H. Zheng, L. Zhang, Y. Li, W. Duan, J. Guo, E. J. Cairns and Y. Zhang, *J. Am. Chem. Soc.*, 2011, **133**, 18522-18525.
24. X. Ji, K. T. Lee and L. F. Nazar, *Nat. Mater.*, 2009, **8**, 500-506.
25. S. S. Zhang and J. A. Read, *J. Power Sources*, 2012, **200**, 77-82.
26. S. Chen, F. Dai, M. L. Gordin and D. Wang, *RSC Advances*, 2013, **3**, 3540-3543.
27. R. Demir-Cakan, M. Morcrette, A. Guéguen, R. Dedryvère and J.-M. Tarascon, *Energy Environ. Sci.*, 2013, **6**, 176-182.
28. D. J. Lee, M. Agostini, J. W. Park, Y. K. Sun, J. Hassoun and B. Scrosati, *ChemSusChem*, 2013, **6**, 2245-2248.

29. L. Ma, K. E. Hendrickson, S. Wei and L. A. Archer, *Nano Today*, 2015, DOI: 10.1016/j.nantod.2015.04.011.
30. W. Zhou, X. Xiao, M. Cai and L. Yang, *Nano Lett.*, 2014, **14**, 5250-5256.
31. C. Wang, X. Wang, Y. Yang, A. Kushima, J. Chen, Y. Huang and J. Li, *Nano Lett.*, 2015, **15**, 1796-1802.
32. Y. Fu, C. Zu and A. Manthiram, *J. Am. Chem. Soc.*, 2013, **135**, 18044-18047.
33. C. Nan, Z. Lin, H. Liao, M.-K. Song, Y. Li and E. J. Cairns, *J. Am. Chem. Soc.*, 2014, **136**, 4659-4663.
34. F. Wu, A. Magasinski and G. Yushin, *J. Mater. Chem. A*, 2014, **2**, 6064-6070.
35. K. Zhang, L. Wang, Z. Hu, F. Cheng and J. Chen, *Sci. Rep.*, 2014, **4**, 6467-6473.
36. L. Chen, Y. Liu, M. Ashuri, C. Liu and L. L. Shaw, *J. Mater. Chem. A*, 2014, **2**, 18026-18032.
37. Z. W. Seh, H. Wang, P.-C. Hsu, Q. Zhang, W. Li, G. Zheng, H. Yao and Y. Cui, *Energy Environ. Sci.*, 2014, **7**, 672-676.
38. Z. W. Seh, J. H. Yu, W. Li, P.-C. Hsu, H. Wang, Y. Sun, H. Yao, Q. Zhang and Y. Cui, *Nat. Commun.*, 2014, **5**, 5017-5024.
39. F. Wu, H. Kim, A. Magasinski, J. T. Lee, H. T. Lin and G. Yushin, *Adv. Energy Mater.*, 2014, **4**, 1400981-1400987.
40. J. D. Peterson, S. Vyazovkin and C. A. Wight, *Macromol. Chem. Phys.*, 2001, **202**, 775-784.
41. X. Chen, H. Li, P. Yin and T. Liu, *Chem. Commun.*, 2015, **51**, 6104-6107.
42. Y. Yang, G. Zheng, S. Misra, J. Nelson, M. F. Toney and Y. Cui, *J. Am. Chem. Soc.*, 2012, **134**, 15387-15394.
43. C. Zu, M. Klein and A. Manthiram, *J. Phys. Chem. Lett.*, 2014, **5**, 3986-3991.
44. K. J. Harry, D. T. Hallinan, D. Y. Parkinson, A. A. MacDowell and N. P. Balsara, *Nat. Mater.*, 2014, **13**, 69-73.
45. J. Song, T. Xu, M. L. Gordin, P. Zhu, D. Lv, Y. B. Jiang, Y. Chen, Y. Duan and D. Wang, *Adv. Funct. Mater.*, 2014, **24**, 1243-1250.
46. K. Cai, M.-K. Song, E. J. Cairns and Y. Zhang, *Nano Lett.*, 2012, **12**, 6474-6479.
47. Z.-G. Yang, R.-M. Ren, X.-Q. Xie and L. Shaw, *Metall. Mater. Trans.*, 1999, **30A**, 1109-1117

## Figures

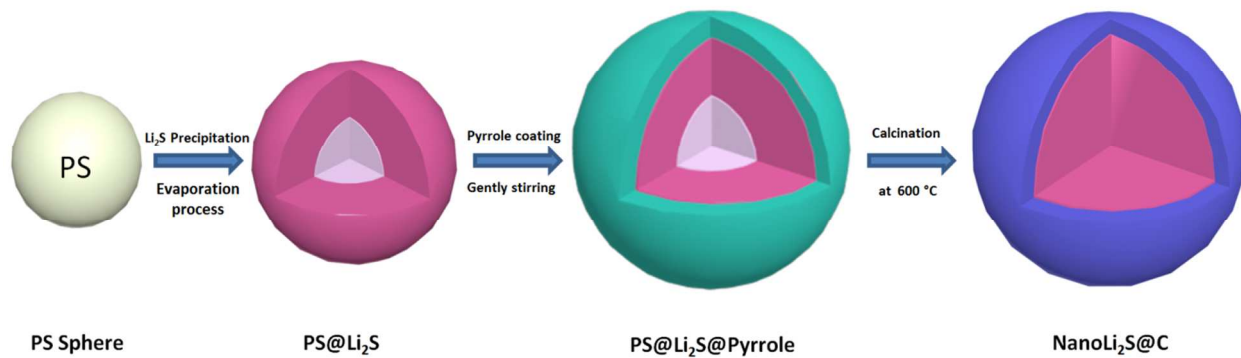


**Figure 1.** Schematic diagram for the formation of nanoLi<sub>2</sub>S@C composites.

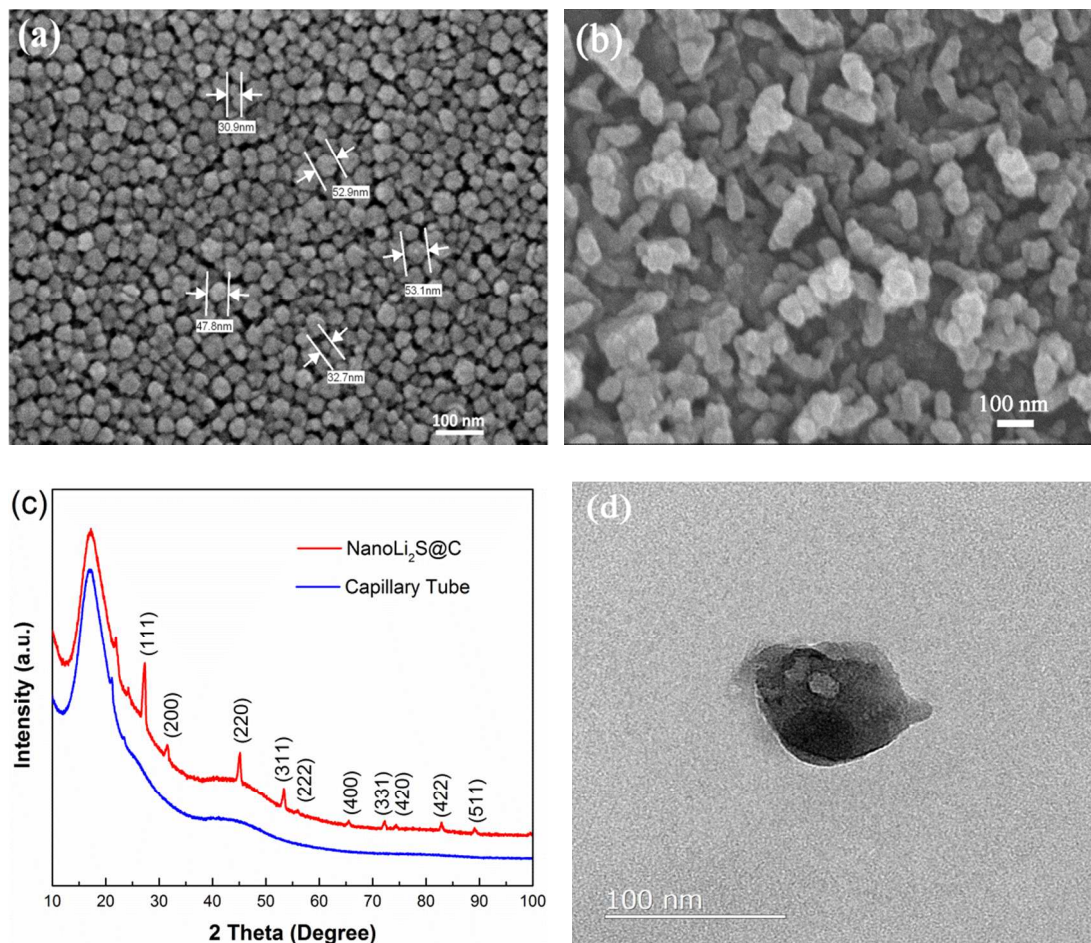


**Figure 2.** (a) FESEM images of polystyrene (PS), (b) FESEM images of nanoLi<sub>2</sub>S@C, (c) XRD pattern, and (d) FETEM image of nanoLi<sub>2</sub>S@C.

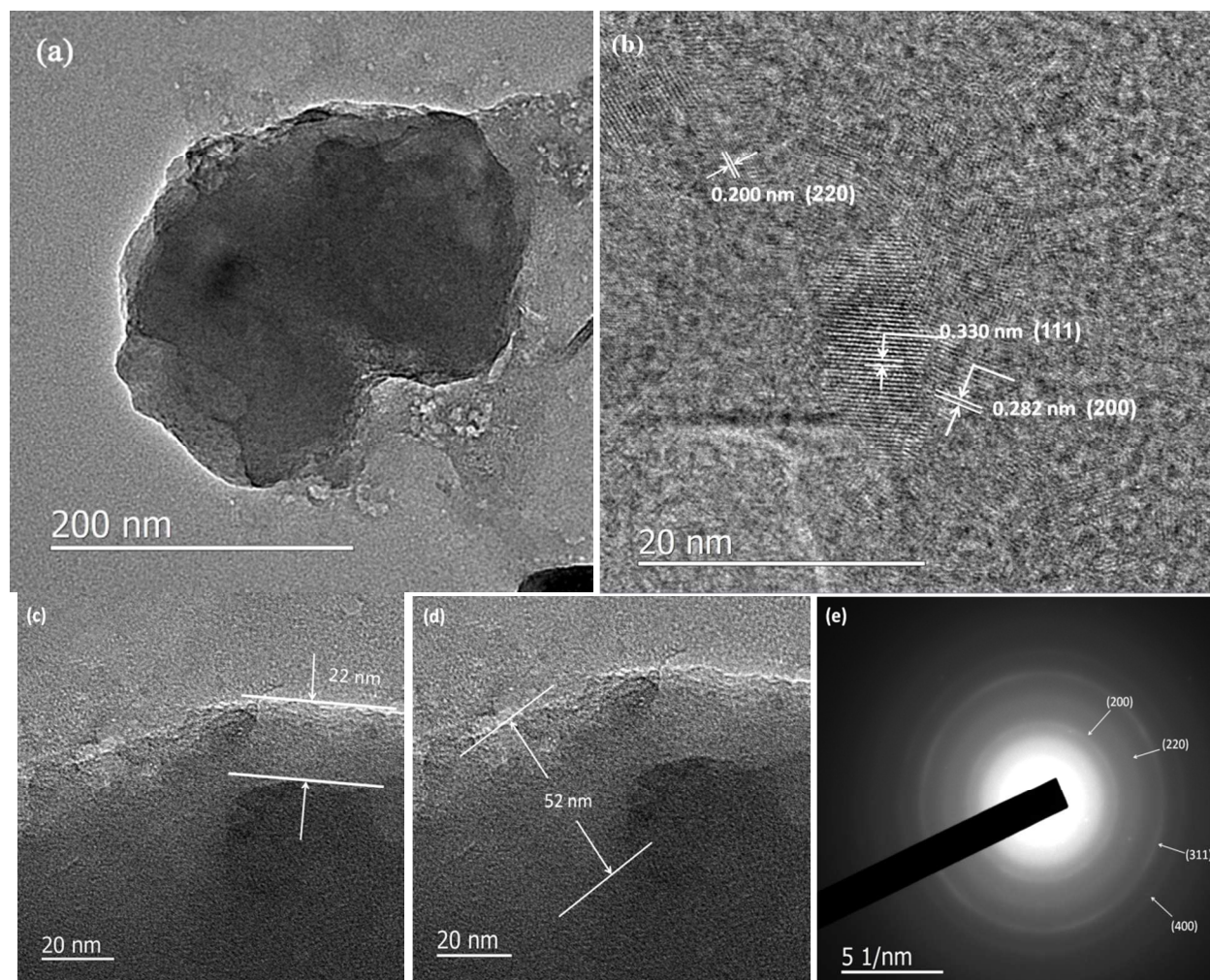


**Figure 3.** Microstructure of the nanoLi<sub>2</sub>S@C nanocomposite: (a) FETEM image, (b-d) TEM images, and (e) selected area diffraction pattern.

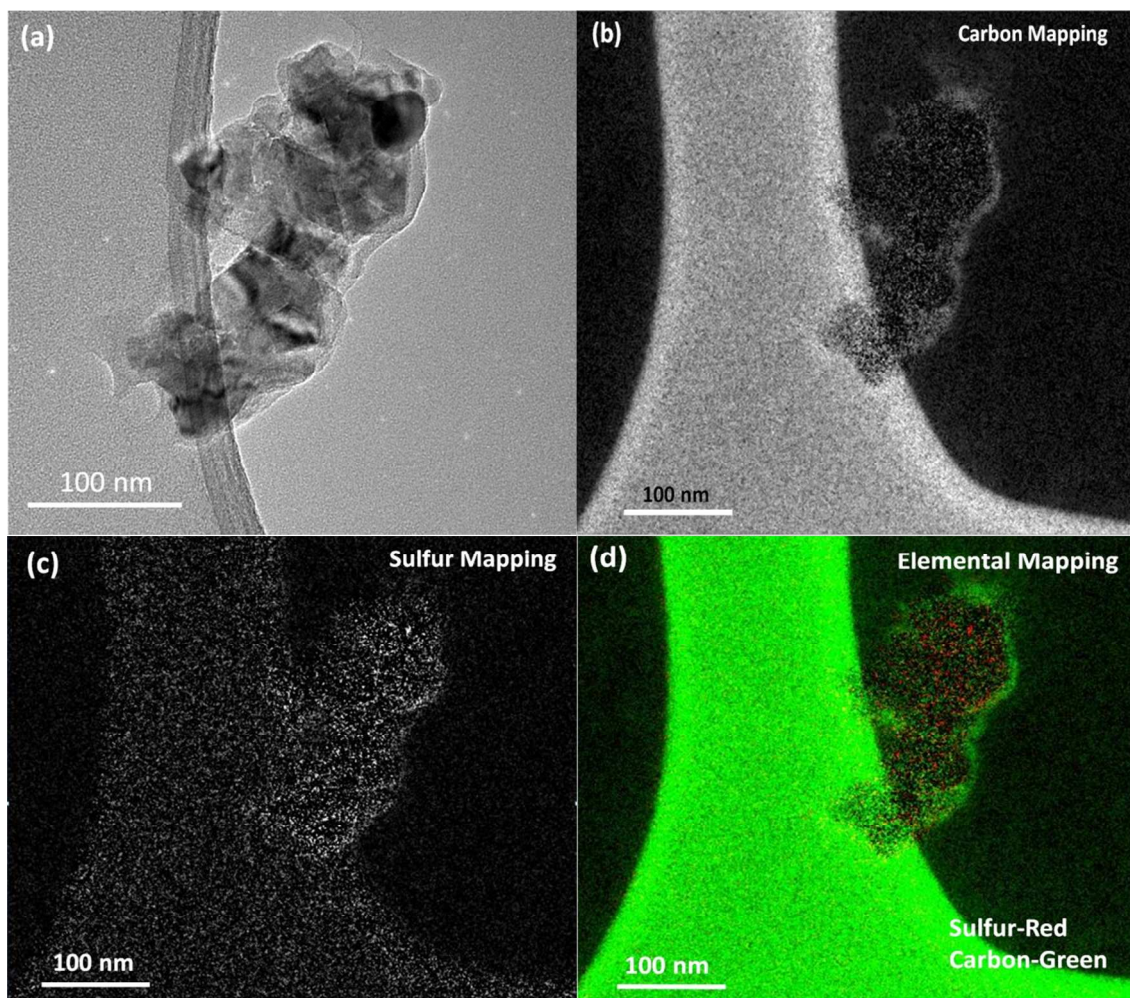


**Figure 4.** (a) FETEM image of nanoLi<sub>2</sub>S@C particles, and their EFTEM elemental mapping with (b) carbon mapping, (c) sulfur mapping, and (d) combined elemental mapping.

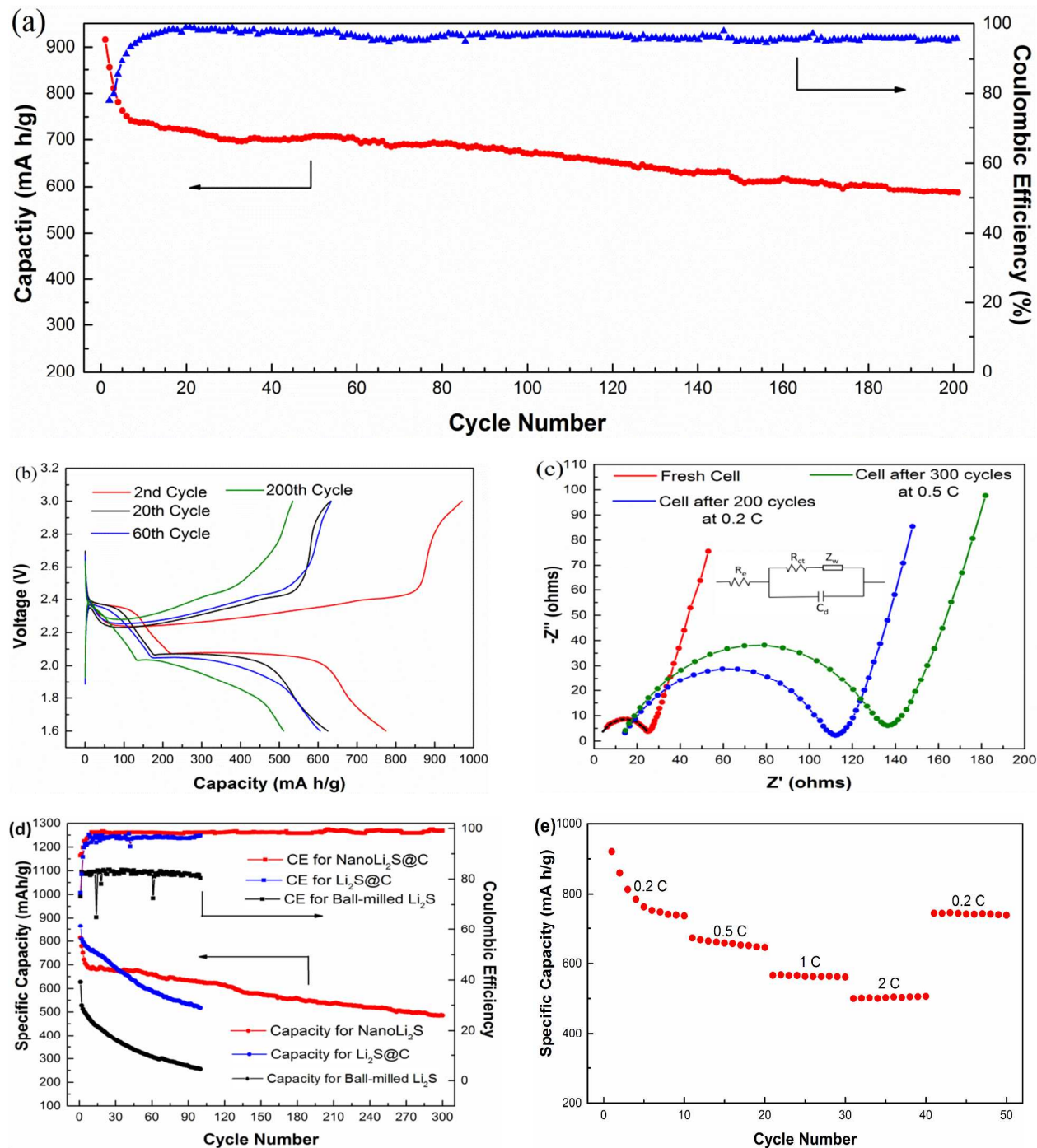


**Figure 5.** (a) Charge-discharge performance at 0.2 C, (b) capacity-voltage profile, (c) EIS of different cells with the equivalent circuit model, (d) cycling results at 0.5 C with comparison to ball-milled Li<sub>2</sub>S and Li<sub>2</sub>S@C, and (e) rate capabilities of the nanoLi<sub>2</sub>S@C half cells.

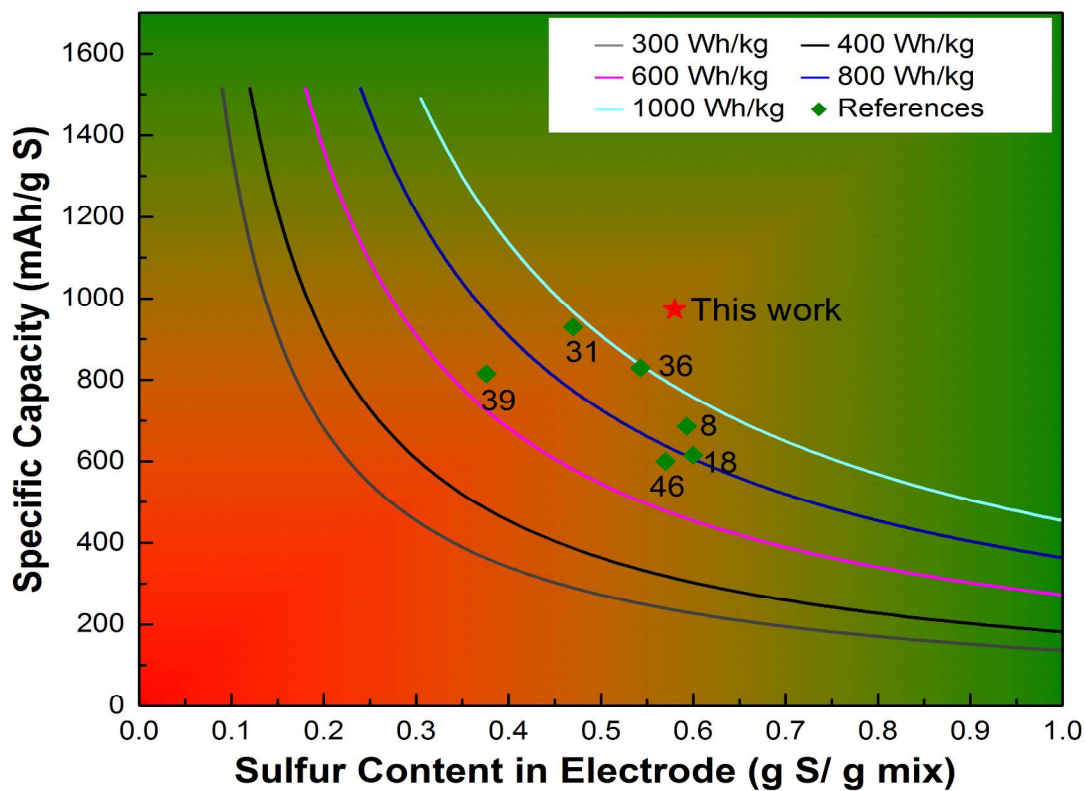


**Figure 6.** Estimated cell specific energy (including all components except for current collector and cell packages) as a function of the specific capacity based on S and the S content of the electrode. The results are based on the data at 100 cycles (except Reference 46 in which the 50th cycle data is used). The previously reported data are marked by green squares for comparison purposes, while this work is highlighted by red star.